Article

The nature of Neanderthal introgression revealed by 27,566 Icelandic genomes

https://doi.org/10.1038/s41586-020-2225-9

Received: 4 July 2019

Accepted: 21 February 2020

Published online: 22 April 2020

Check for updates

Laurits Skov[1,2,7]✉, Moisès Coll Macià[1,7], Garðar Sveinbjörnsson[3], Fabrizio Mafessoni[2], Elise A. Lucotte[1], Margret S. Einarsdóttir[3], Hakon Jonsson[3], Bjarni Halldorsson[3,4], Daniel F. Gudbjartsson[3], Agnar Helgason[3,5], Mikkel Heide Schierup[1]✉ & Kari Stefansson[3,6]✉

Human evolutionary history is rich with the interbreeding of divergent populations. Most humans outside of Africa trace about 2% of their genomes to admixture from Neanderthals, which occurred 50–60 thousand years ago[1]. Here we examine the effect of this event using 14.4 million putative archaic chromosome fragments that were detected in fully phased whole-genome sequences from 27,566 Icelanders, corresponding to a range of 56,388–112,709 unique archaic fragments that cover 38.0–48.2% of the callable genome. On the basis of the similarity with known archaic genomes, we assign 84.5% of fragments to an Altai or Vindija Neanderthal origin and 3.3% to Denisovan origin; 12.2% of fragments are of unknown origin. We find that Icelanders have more Denisovan-like fragments than expected through incomplete lineage sorting. This is best explained by Denisovan gene flow, either into ancestors of the introgressing Neanderthals or directly into humans. A within-individual, paired comparison of archaic fragments with syntenic non-archaic fragments revealed that, although the overall rate of mutation was similar in humans and Neanderthals during the 500 thousand years that their lineages were separate, there were differences in the relative frequencies of mutation types—perhaps due to different generation intervals for males and females. Finally, we assessed 271 phenotypes, report 5 associations driven by variants in archaic fragments and show that the majority of previously reported associations are better explained by non-archaic variants.

Eurasians are estimated to trace around 2% of their genomes to introgression from archaic humans[2] related to the Vindija Neanderthal[1]. In Europeans, archaic ancestry is consistent with contributions by a single population of Neanderthals[3] through one or more pulses[4–7]. As many archaic fragments still segregate in contemporary populations, it follows that archaic genomes can be partially mined from whole-genome sequence data from Europeans. Once such archaic fragments are identified, it is possible to determine the effect that variants in these fragments have on phenotypic diversity in modern humans[8–13].

Previous attempts to identify archaic fragments in contemporary humans have generally relied on existing archaic genomes[14–16], which partially represent the haplotypic diversity of the archaic populations. Moreover, the introgressing Neanderthals were probably from populations that were separated both in time and space from the three archaic individuals who have so far been sequenced to high coverage—hereafter referred to as DAV (Denisovan, Altai Neanderthal and Vindija Neanderthal)[1,17,18]. Some archaic fragments in contemporary humans will be missed by methods that depend on DAV genomes. Even more would be missed if the genetic information of introgressing Neanderthals is not well represented by one of the DAV genomes, for example, owing to admixture between archaic groups[18,19]. Here we investigated the archaic diversity in contemporary Europeans and its relationship to the DAV genomes.

A diverse set of introgressed fragments

We used a two-state hidden Markov model that is not conditioned on DAV genomes[20] to search for archaic fragments independently in 55,132 haploid genomes from 27,566 sequenced Icelanders that were sequenced to 30X and accurately phased using long-range phasing[21] (Supplementary Information 1, 2.1). The model detects fragments with a high density of derived alleles that were not found in an outgroup population of 292 sub-Saharan Africans (hereafter referred to as Africans) from the 1000 Genomes Project[22]. For all subsequent analyses, we retained 14,422,595 fragments with a posterior probability of more than 90% of being archaic (Supplementary Information 2). This threshold was used because simulations indicate that our model has a false-positive rate of less than 4% while still recovering around 71.5% of all archaic sequences per haploid genome (Extended Data Fig. 1 and Supplementary Information 2.3, 3.2).

The archaic fragments carried derived alleles at 395,304 single-nucleotide polymorphisms (SNPs) that are absent in Africans (Supplementary Data 1). Of these variants, 147,925 were found in the

[1]Bioinformatics Research Centre, Aarhus University, Aarhus, Denmark. [2]Max Planck Institute for Evolutionary Anthropology, Leipzig, Germany. [3]deCODE Genetics, Amgen, Reykjavik, Iceland. [4]School of Science and Engineering, Reykjavik University, Reykjavik, Iceland. [5]Department of Anthropology, University of Iceland, Reykjavik, Iceland. [6]Faculty of Medicine, School of Health Sciences, University of Iceland, Reykjavik, Iceland. [7]These authors contributed equally: Laurits Skov, Moisès Coll Macià. ✉e-mail: laurits_skov@eva.mpg.de; mheide@birc.au.dk; kari.stefansson@decode.is

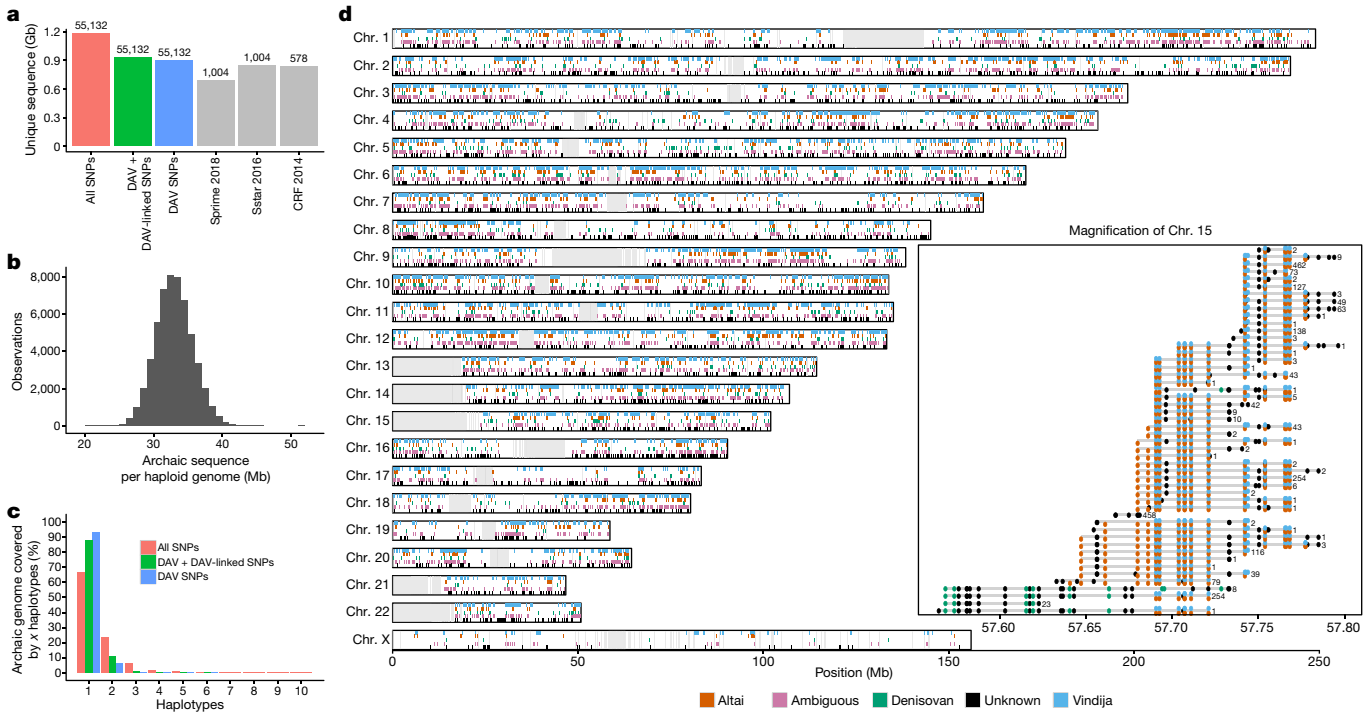

Fig. 1 | Archaic diversity in 55,132 Icelandic haploid genomes. a, The total length of the genome covered by archaic fragments using: all SNPs, DAV-linked and DAV SNPs, and only DAV SNPs. The amount of archaic sequences from previous studies based on the 1000 Genomes Project is also shown (Sprime[3], Sstar[14] and CRF[15]). Sample sizes are shown above the bar. **b**, The distribution of the average amount of archaic sequences per haploid genome. **c**, Fraction of the introgressing genome covered by different numbers of haplotypes. We classify fragments into groups of haplotypes for which the mean difference between fragments in the cluster is less than 1 difference per 10 kb. We do this for all SNPs, DAV-linked and DAV SNPs, and DAV SNPs. **d**, The genome-wide distribution of archaic haplotypes, coloured according to the DAV genome that they are closest to. Unknown, no derived alleles shared with a DAV genome; ambiguous, alleles that are equidistant to more than 1 DAV genome. The inset shows a 225-kb region on chromosome 15 that has a high fragment diversity. SNPs are coloured according to the DAV genome that they are found in; non-DAV and DAV-linked/unlinked SNPs are shown in black. The absolute frequency of each fragment is shown on the right. Some fragments appear to be Denisovan, while others are a mosaic of Denisovan and Neanderthal.

DAV genomes (hereafter DAV variants). These variants and the fragments that carried them are very likely to be archaic in origin[23]. The remaining 247,379 SNPs have derived alleles that were not observed in the DAV genomes. Some may have been present in introgressing Neanderthals, but are not captured by the three DAV genomes. Others could have arisen on archaic fragments in humans after the introgression. The remainder are non-archaic variants that were not observed in our African reference set. Archaic variants that are not observed in the DAV genomes are expected to be in strong linkage disequilibrium with DAV variants from the same archaic fragments. Of the 247,379 putative archaic variants, 47,193 were found to be linked ($r^2 > 0.9$) to at least one nearby DAV variant (DAV-linked variants), whereas 145,153 were found on fragments with DAV variants but were not linked to them. The latter DAV-unlinked variants tend to have a lower frequency than DAV and DAV-linked variants, suggesting that many of the underlying mutations occurred on archaic fragments after Neanderthal introgression (Extended Data Fig. 2a). The remaining 55,033 variants were found on putative archaic fragments with no DAV variants and are hereafter called nonDAV variants.

As introgressing archaic variants must be at least 50 thousand years old, they have a greater chance of being found in multiple populations than non-archaic variants of the same frequency. Both DAV-unlinked and nonDAV variants are found less often in European populations from the 1000 Genomes Project (55% and 64%, respectively) (Extended Data Fig. 2b) than DAV and DAV-linked variants (84% and 77%, respectively) after controlling for allele frequency. This is consistent with fewer DAV-unlinked and nonDAV variants having an archaic origin. DAV-unlinked variants are closer to the ends of putative archaic fragments than DAV variants: 12.3 kilobases (kb) compared with 26.8 kb median distance from the edge (Wilcoxon signed-ranked test, $P < 2.2 \times 10^{-16}$) (Supplementary Fig. 2.5.3), indicating a slight increase in false positives at the ends of fragments.

The 14,422,595 candidate archaic fragments correspond to 112,709 unique fragments (based on start–end positions), have a combined length of 1,818 Gb and cover 1.179 Gb (48.2%) of the callable genome (2.445 Gb) (Fig. 1a), exceeding previous studies using Sprime (0.688 Gb)[3], Sstar (0.846 Gb)[24] and CRF (0.834 Gb)[15] (Fig. 1a). After pruning fragments to start and end with DAV-linked and DAV variants, archaic coverage is estimated to be 0.962 Gb (39.3% of the callable genome, spanned by 59,124 unique fragments). The most conservative estimate of archaic coverage, based on ends defined by only DAV variants, is 0.929 Gb (38% of the callable genome, spanned by 56,388 unique fragments) (Fig. 1a and Supplementary Table 2.4.1). Even after analysing 55,132 haploid genomes, it may be deduced that not all archaic fragments have been detected in Icelanders (Supplementary Figs. 2.4.3, 2.5.4), and even more remain to be found in other populations.

An average of 261.6 archaic fragments, corresponding to around 33 Mb, were identified per haploid genome (Fig. 1b and Supplementary Information 2.3). Callable positions in the genome were, on average, covered by 743 archaic fragments, corresponding to an average frequency of 1.34% in the 55,132 haploid genomes analysed. These are probably underestimates, because our method misses archaic fragments that are short or not sufficiently divergent from non-archaic fragments. Simulations suggest a false-negative rate of 28.5%, suggesting that the frequency of archaic fragments may be closer to 1.9% (Supplementary Information 3.2).

The average nucleotide diversity between overlapping archaic fragments, when considering DAV and DAV-linked variants is 2.00×10^{-5}

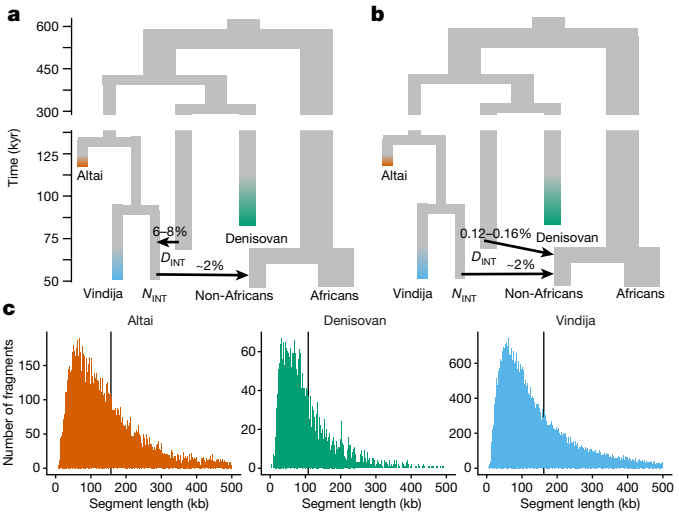

Fig. 2 | Phylogenetic relationships of archaic fragments to sequenced archaic genomes. Throughout this figure Vindija is shown in blue, Altai in red and Denisova in green. D_{INT}, introgressing Denisovan population; N_{INT}, introgressing Neanderthal population. Branch thickness in the phylogenetic trees reflects the effective population size, in which the human ancestral branch is 10,000. Split times were obtained from a previous study[1] and the N_e is calculated according to Supplementary Information 2.7.2. **a**, **b**, Two different scenarios to account for the presence of Denisovan fragments in contemporary Icelanders are shown. **a**, Denisovan introgression into Neandertals is followed by Neanderthal introgression into humans. **b**, Direct Denisovan introgression into the ancestor of all non-Africans. kyr, thousand years ago. **c**, Length distribution of Altai, Denisovan and Vindija fragments. The dashed lines indicate the mean segment lengths. Altai Neanderthal, length = 157 ± 1.045 kb; Denisovan, length = 108 ± 1.498 kb; Vindija Neanderthal, length = 162 ± 0.626 kb; lengths are mean ± s.e.m.

(95% confidence interval, 1.86×10^{-5}–2.12×10^{-5}), which is similar to the heterozygosity in Neanderthals (Altai Neanderthal, 1.63×10^{-5}; Vindija Neanderthal, 1.71×10^{-5}) and the Altai Denisovan (1.89×10^{-5})[1]. Some genomic regions contained highly diverse archaic fragments indicative of multiple introgressing haplotypes (Extended Data Fig. 3). To shed light on the number of archaic individuals who contributed to contemporary humans, we clustered overlapping fragments and divided them into subgroups that did not exceed a mean pairwise distance of 1 variant per 10 kb (Supplementary Information 5). We postulate that each subgroup approximates a different introgressing archaic haplotype. When only DAV and DAV-linked variants were used to define subgroups, the percentage of fragments assigned to just one subgroup is 88.1% (Fig. 1c and Supplementary Information 5.2), which increases to 93.2% using only DAV variants. However, even with such stringent criteria, we find genomic regions with up to six different archaic haplotypes—indicating that multiple archaic individuals were involved in the introgression (Supplementary Fig. 5.1.1).

Figure 1d shows the genomic distribution of archaic fragments and the DAV genome that they share the most variants with: Vindija Neanderthal (50.8%), Altai Neanderthal (13.1%), Denisovan (3.3%), two or more DAV genomes (20.4%) or not shared with a DAV genome (unknown, 12.2%). Fragments of unknown origin are longer (mean = 77.9 kb, s.e.m. = 0.5 kb) than false-positive archaic fragments in simulations (mean = 40.7 kb, s.e.m. = 0.7 kb) (Extended Data Fig. 1 and Supplementary Information 3.2). However, a higher false-positive rate for unknown fragments is suggested by a shorter mean coalescence time to sub-Saharan Africans (34,130 generations, s.e.m. = 136 generations) than for archaic fragments that contain DAV variants (38,318 generations, s.e.m. = 48 generations) (Wilcoxon signed-ranked test, $P < 2.2 \times 10^{-16}$) (Extended Data Fig. 4). Because our method of detection is not dependent on existing archaic genomes, we are able to detect mosaic fragments that switch similarity with different DAV genomes along their length. Figure 1d shows an example of a mosaic fragment, with multiple Denisovan-specific derived alleles in the first 250 kb, followed by Altai-specific variants (Supplementary Figs. 2.6.4–2.6.10). We find that 18.9% of fragments are mosaic.

Both our results and previous studies[1] indicate that the introgressing Neanderthal was closer to the Vindija Neanderthal than the Altai Neanderthal or Denisovan. However, our method yields many long fragments that are most closely related to the Altai Neanderthal and Denisovan genomes (Fig. 2c) and some previous studies have also reported such fragments in Europeans[3,20,23]. One possible explanation is introgression from groups with genomes that are related to the Denisovan and Altai genomes into introgressing Neanderthals before this group contributed to modern human genomes. Alternatively, the introgressing Neanderthals could have been a Vindija-like group that carried some anciently diverged haplotypes due to incomplete lineage sorting that now seem, by chance, to be more similar to the Altai and Denisovan genomes than the Vindija genome. To resolve the origin of these archaic fragments, we performed extensive simulations under different demographic and admixture models (Supplementary Information 3.3 and Supplementary Fig. 3.1.1). The results indicate that the observed characteristics of Denisovan-like fragments in Icelanders are not compatible with a simple introgression from a Vindija-like group without that population having had prior admixture with a Denisovan-like group (Supplementary Information 3.3.3 and Supplementary Fig. 3.1.1). An equally intriguing scenario that cannot be ruled out is direct admixture from a Denisovan-like group into the common ancestors of non-Africans before the main Neanderthal admixture event (Fig. 2a, b).

We estimated the effective population sizes (N_e) of different archaic groups using pairwise differences between the archaic fragments identified in Icelanders and the high-coverage DAV genomes (Supplementary Information 2.7) and divergence times estimated in previous studies[1,18] (Supplementary Information 2.7.2). We find that Neanderthals had a relatively small N_e of 2,000–3,000 individuals, in agreement with previous pairwise sequential Markov chain analyses of Neanderthal genomes[1].

Our greater sample size (n = 27,566 compared with n = 502 in the 1000 Genomes Project) enables a more fine-scale identification of genomic regions with very little or no archaic introgression (archaic deserts). Searching for 1-Mb windows with no fragments containing DAV variants, we found 282 distinct archaic deserts covering 570 Mb (23.3% of the callable genome) (Extended Data Fig. 5 and Supplementary Data 4). The X chromosome is particularly devoid of archaic introgression as previously reported[15] (Fig. 1d). The archaic deserts are slightly more gene dense (7.52 ± 0.372 genes per Mb) than non-deserts (6.87 ± 0.179 genes per Mb) (Wilcoxon signed-ranked test, P = 0.043). They also have lower mean recombination rates (0.894 cM per Mb, s.e.m. = 0.031) than non-deserts (1.36 cM per Mb, s.e.m. = 0.02) (Wilcoxon signed-ranked test, $P < 2.2 \times 10^{-16}$) (Extended Data Fig. 5), also after adjusting for gene density (Supplementary Fig. 4.2.1). Furthermore, the proportion of archaic fragments spanned by DAV-linked and DAV variants was higher in regions with a greater recombination rate (Spearman's ρ = 0.15, $P = 4.4 \times 10^{-54}$) and the nucleotide diversity of archaic fragments was also higher in these regions (Spearman's ρ = 0.18, $P = 1.3 \times 10^{-79}$) (Extended Data Fig. 6). Taken together, these observations indicate that non-deleterious archaic variants were more likely to be retained in the human gene pool when they could be uncoupled from deleterious archaic variants by recombination[25].

Mutation processes in archaic fragments

The rate and types of mutation are influenced by several factors that may differ between human populations and between great-ape species[26]. The fully phased Icelandic genomes allow us to compare syntenic archaic and non-archaic fragments from the same individual

to determine whether differences in mutational processes existed between humans and Neanderthals during the approximately 500,000 years of divergence before archaic introgression (*T* in Fig. 3a; Supplementary Information 6.1). We calculated the mean difference in the number of derived alleles (including those shared with Africans) between the paired archaic and non-archaic fragments (Δ_{AH}, Supplementary Information 6.2). We modelled the ascertainment bias of the hidden Markov model approach used to identify archaic fragments, which is predisposed towards SNP-dense fragments (Supplementary Information 3.4.1), thereby inflating the Δ_{AH} particularly at the edges of fragments (Supplementary Information 3.4.2, 6.2.1). We compared the observed Δ_{AH} in Icelandic genomes with multiple simulated scenarios of increasing differences in the density of archaic-to-human SNPs (Fig. 3b and Supplementary Information 3.4.1). Although the best-fitting scenario corresponds to a 2% higher SNP density in archaic fragments (Extended Data Fig. 7), given the uncertainties associated with the parameters used in the coalescent simulations and variance among replicates of the same scenario, we do not find a greater mutation rate in the Neanderthal lineage before the introgression event.

We next compared the mutation spectrum between the paired archaic and non-archaic fragments. A set of non-overlapping fragments was used to avoid counting the same derived allele multiple times (Supplementary Information 6.1) and we trimmed 15 kb from both ends of all fragments to avoid edge effects (Supplementary Information 6.3.1). We classified mutations as ancestral-to-derived alleles and collapsed the strand complement mutation counts into seven distinct mutational types, separating CpG>TpG from C>T, as the latter mutation type is thought to evolve in a more clock-like manner[27]. The archaic:non-archaic proportional ratio (Fig. 3c, Supplementary Data 7 and Supplementary Information 6.3.2) revealed more C>G and fewer T>C and CpG>T variants in archaic fragments than in their non-archaic counterparts. Notably, the most-extreme ratios are observed for C>G and CpG>T variants, which have the lowest (1:1) and highest (6:1) paternal-to-maternal age effect ratios for de novo mutations in contemporary humans (the mean ratio across all types is 3:1)[28]. These differences are consistent with mothers having been older and fathers younger in the Neanderthal lineage than in the human lineage, although other causes cannot be ruled out. The C>G enrichment in archaic fragments is not due to an excess of archaic fragments in the C>G-cluster-enriched regions[28]. Furthermore, the differences in mutational types are robust to several conservative filtering schemes and are therefore probably not due to false-positive archaic fragments (Supplementary Information 6.3.2 and Supplementary Data 7). We next expanded the classification of each mutation type, including their 5′ and 3′ base-pair context, resulting in 96 distinct mutational types (Fig. 3d and Supplementary Data 7). Five types (CCT>G, CCC>G, CTG>G, TCC>A and CCA>G) were overrepresented in archaic fragments after Bonferroni adjustment, three of which involved C>G mutations.

It has been suggested[29–31] that Neanderthals accumulated more deleterious mutations than humans because of less efficient selection due to a smaller N_e. We did not find an excess of deleterious variants in the archaic fragments identified in Icelanders (χ^2 test, $P = 0.71$) (Fig. 3e and Supplementary Table 6.4.1), after comparing their distribution across four functional impact categories (lowest, low, moderate and high) that were obtained from the Variant Effect Predictor[32] (Supplementary Information 6.4). Therefore, if introgressing Neanderthal fragments had more deleterious variants at the time of introgression, these have already been removed by purifying selection.

Phenotypic effects of archaic fragments

To study the influence of archaic variants on the phenotypic diversity of contemporary humans, we examined their association with 271 traits based on around 32 million variants called and imputed for 214,192 Icelanders (Supplementary Information 7.1). In the first step of filtering

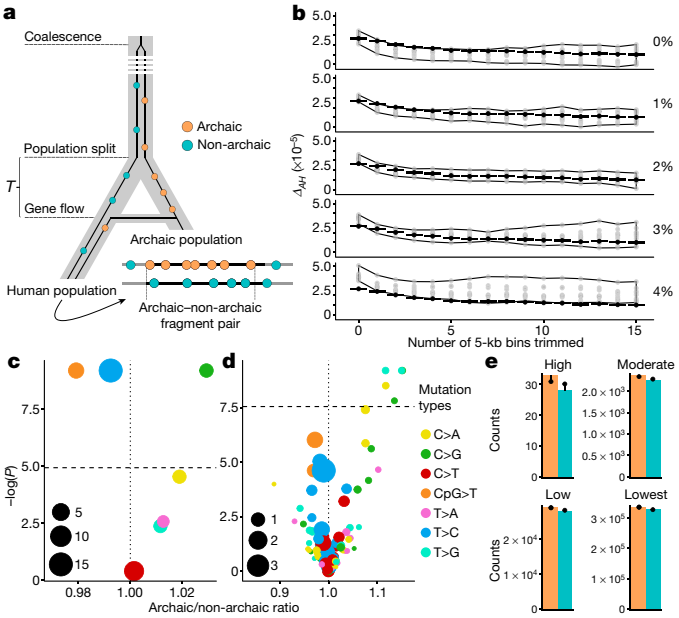

Fig. 3 | Comparison of the rate, spectrum and influence of mutations on archaic and non-archaic fragments. a, The phylogenetic tree connecting human and archaic populations (grey bands). The black lines in the tree represent coalescence paths of an archaic and a non-archaic fragment pair in an Icelander. Circles represent mutations (derived alleles) that accumulated on non-archaic (blue) and archaic (orange) fragments. *T* refers to the time these two fragments were isolated in human and archaic ancestral groups. The two horizontal lines with mutations illustrate the paired fragments sampled. **b**, Comparison of the observed Icelandic Δ_{AH} (black dots with 95% confidence intervals) with expectations based on 10 replicates (grey dots) of simulations of increasing Neanderthal-to-human mutation rate percentages (as indicated on the right). Wide bands show the maximum and minimum Δ_{AH} among the 10 replicates per scenario. Results are based on trimming 0–15 5-kb bins from fragment ends (*x* axis). Only fragments ≥100 kb are used. **c**, The archaic/non-archaic proportional ratio (*x* axis) of the number of derived alleles against the *P* value (two-sided permutation test, *y* axis) for each of seven different mutation types (represented by different colours). The size of each point shows the mean archaic and non-archaic fragment sample size for each mutation type ($\times 10^4$, sample sizes are included in Supplementary Data 7). The horizontal dashed line shows the Bonferroni-adjusted significance threshold and the vertical dashed line indicates a ratio of 1 (no enrichment). **d**, The same as **c**, but subdividing mutation types according to the 96-mutation type spectrum. **e**, Observed counts of derived alleles from human (blue) and archaic (orange) fragments based on four categories of functional impact. The χ^2-expected counts are denoted as black points and the black lines indicate the difference from the observed counts.

(Fig. 4a), we evaluated the association of the 395,304 archaic-derived alleles with each of 271 phenotypes using genome-wide significance thresholds based on functional effects (such as, exon, intron and intergenic regions)[33]. This yielded 4,361 archaic phenotype-associated variants, corresponding to 651 independent association signals after accounting for linkage disequilibrium between them.

In the second step of filtering, we tested whether any correlated ($r^2 > 0.2$) non-archaic variant within a 2-Mb radius better accounted for an association than the strongest archaic candidate variant. For 550 association signals, we found a non-archaic variant in high linkage disequilibrium with the strongest archaic candidate. Of these, 431 involved a non-archaic variant with a substantially stronger association (>10-fold) with the phenotype in question. For 33 cases, the non-archaic variant had a stronger association (≤10-fold) with the phenotype. In another 86 instances, archaic variants were disregarded because a highly correlated ($r^2 > 0.9$) non-archaic variant with a slightly stronger association was identified. This left 101 archaic variants.

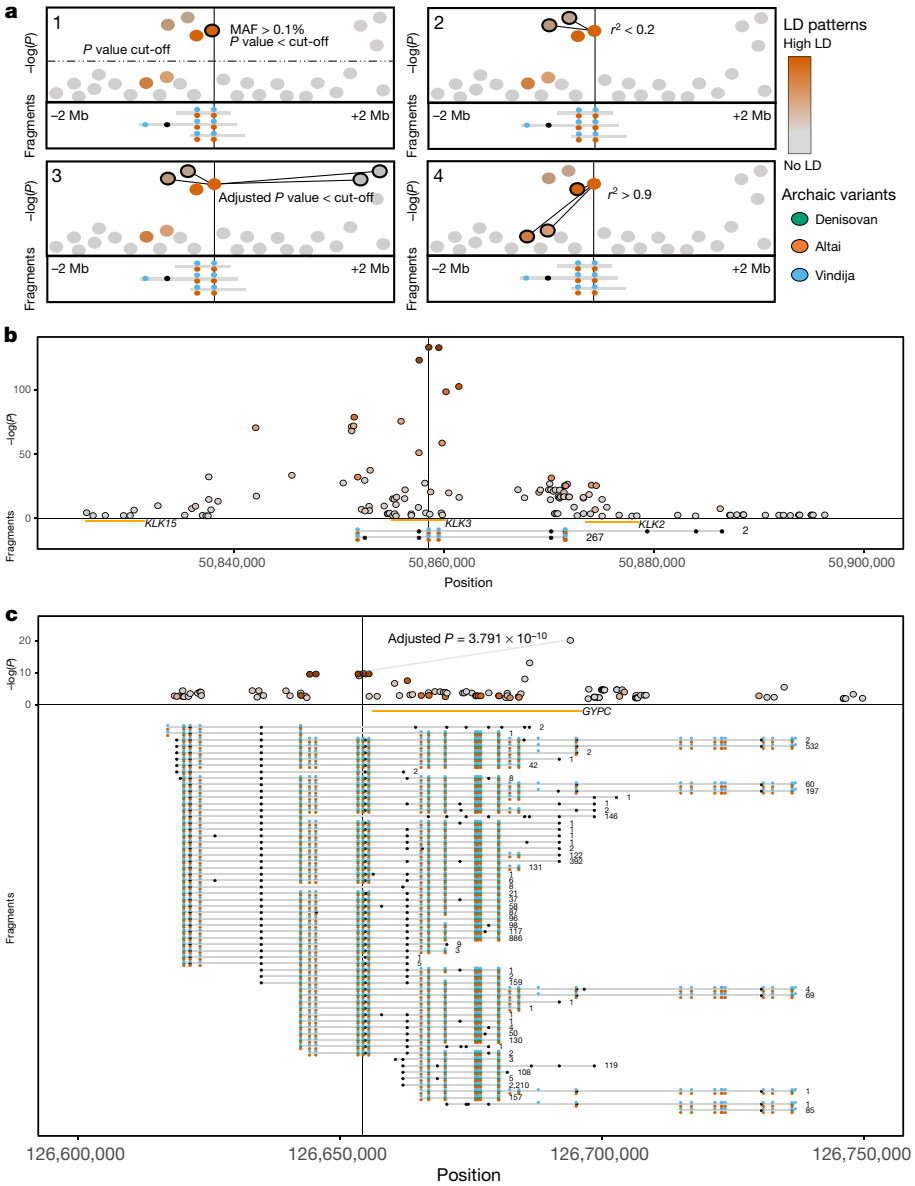

Fig. 4 | Phenotype association with archaic variants. a, Procedure to determine whether genotype–phenotype associations are due to archaic variants. Each subpanel shows a 4-Mb region on the *x* axis and is divided into two frames. In the top frame, the *y* axis shows the $-\log_{10}$-transformed values of the association *P* value for variants in the region coloured by their linkage disequilibrium (LD) to the candidate variant, which is marked by a vertical line. All archaic variants are outlined. The bottom frame shows the archaic fragments (grey) punctuated by archaic variants (Altai, orange; Vindija, blue; Denisovan, green; other, black). (1) We selected all archaic variants with an association *P* value under the genome-wide significance threshold and a minor allele frequency (MAF) above 0.1%. (2) The candidate archaic variant is rejected as the cause of the association if there is a non-archaic variant with a stronger association to the phenotype with $r^2 > 0.2$ to the candidate archaic variant. (3) We reject the variant if the *P* value of the candidate variant drops below the genome-wide significance threshold after conditioning on a non-archaic variant with a lower *P* value within a 2-Mb radius. (4) We reject candidates that are not in strong linkage disequilibrium ($r^2 > 0.9$) with at least one other archaic variant from the same fragment. **b**, Association of an archaic variant (rs17632542) on chromosome 19 with prostate-specific antigen. The top frame shows association *P* values for all variants in the region, coloured according to their linkage disequilibrium with the candidate archaic variant. The bottom frame shows genes (orange) and archaic fragments as described for **a**. **c**, Association of an archaic variant (rs28387074) on chromosome 2 with mean corpuscular haemoglobin concentration (as described for **b**). Although another non-archaic variant in the same region has a lower *P* value, the association of the candidate variant remains significant after adjustment.

In the third step, we tested whether the archaic variants remained genome-wide significant after conditioning on non-archaic variants within a 2-Mb radius with a stronger association to the phenotype. This analysis left 64 archaic variants.

Finally, we pruned variants that were not in high linkage disequilibrium with other archaic variants ($r^2 > 0.9$), leaving only five independent archaic variants likely to be a true source of phenotypic association (Supplementary Data 8). One is an example of a strong association with a reduced level of prostate-specific antigen driven by rs17632542 (the derived allele of which is found in Altai and Vindija Neanderthals), which has been reported to reduce the risk of prostate cancer; however, the introgressed status of the variants was not reported[34] (Fig. 4b). Another is rs28387074, which decreases the concentration of haemoglobin and survives adjustment for non-archaic variants that are responsible for another strong signal in the same region (Fig. 4c). The remaining three association signals due to archaic variants are for reduced height (rs3118914), decrease in mean corpuscular haemoglobin (rs72728264) and an increase in plasma prothrombin time (rs6013) (Supplementary

Data 8). Two of the association signals (rs3118914 and rs72728264) are DAV-unlinked variants that are in strong linkage disequilibrium ($r^2 > 0.9$) with other DAV-unlinked variants.

We also assessed 30 previously reported phenotypic associations with archaic variants[12,13,15]. In four cases, we did not have a sufficiently similar phenotype to test. For the remaining 26 associations, 10 were not nominally significant ($P > 0.05$) in our genome-wide association studies and 13 lost significance when conditioned on a nearby non-archaic variant that was more likely to be the true source of the association (Supplementary Data 8). These non-archaic variants are present in African populations, have a greater effect on the phenotype and a lower *P* value than the originally reported 13 archaic variants (Supplementary Figs. 7.1.6–7.1.10). We could therefore only validate the archaic origin of 3 out of 26 previously reported association findings attributed to archaic variants (Supplementary Data 8). This highlights the importance of considering flanking non-archaic variants when assigning an archaic origin to a phenotype association. To assess the genome-wide effect of archaic introgression on phenotype variation, we also counted the number of archaic-derived alleles carried by each contemporary Icelander and tested this polygenic score of archaic ancestry for association with each of the 271 phenotypes. In the case of height, for example, this test would reveal whether the surviving fragments from archaic introgression resulted in taller or shorter contemporary Icelanders. After adjusting for the number of tests, we found no evidence for association between the polygenic score and any of the 271 tested phenotypes (Supplementary Data 8), indicating that archaic ancestry has—at most—a modest directional impact on contemporary human phenotype variation.

Discussion

We show that a large part of an archaic genome can be mined from contemporary descendants of populations that were recipients of introgression around 50–60 thousand years ago. The recovered archaic fragments are consistent with being descended from multiple archaic individuals, who belonged to an archaic population similar to the Vindija Neanderthal. However, the considerable proportion of archaic fragments that are closer to the Denisovan genome cannot be explained by incomplete lineage sorting (Supplementary Information 3.3.3.1). Rather, they require Denisovan introgression, either directly into humans or into Neanderthals who later mixed with humans, which must have occurred soon after they migrated out of Africa, because its signal is found in all contemporary non-African populations from the Simons Genome Diversity Project (Supplementary Information 5.2). This raises the possibility that there were Denisovan-like groups west of the Altai mountains, where such gene flow into humans must have occurred. This is consistent with growing evidence of extensive population movements towards the end of Neanderthal history both in Europe[35] and in the Altai mountains[19]. Hopefully, additional archaic genomes will shed light on this complex history of interbreeding between hominin groups.

The similar mutation rates in Neanderthals and modern humans imply that the apparent slowdown in the human mutation rate[36] is unlikely to have occurred between 500,000 and 55,000 years ago. However, differences in the mutation spectrum of archaic and non-archaic fragments raise the possibility of long-term differences in male and female generation intervals between the species. Finally, our most far-reaching conclusion is that archaic introgression has a relatively minor effect on phenotypic variation in contemporary humans. Given the non-random genomic distribution of archaic fragments in contemporary Icelanders, it follows that this influence must have been greater in the past.

Online content

Any methods, additional references, Nature Research reporting summaries, source data, extended data, supplementary information, acknowledgements, peer review information; details of author contributions and competing interests; and statements of data and code availability are available at https://doi.org/10.1038/s41586-020-2225-9.

1. Prüfer, K. et al. A high-coverage Neandertal genome from Vindija Cave in Croatia. *Science* **358**, 655–658 (2017).
2. Fu, Q. et al. Genome sequence of a 45,000-year-old modern human from western Siberia. *Nature* **514**, 445–449 (2014).
3. Browning, S. R., Browning, B. L., Zhou, Y., Tucci, S. & Akey, J. M. Analysis of human sequence data reveals two pulses of archaic Denisovan admixture. *Cell* **173**, 53–61 (2018).
4. Wall, J. D. et al. Higher levels of Neanderthal ancestry in East Asians than in Europeans. *Genetics* **194**, 199–209 (2013).
5. Kim, B. Y. & Lohmueller, K. E. Selection and reduced population size cannot explain higher amounts of Neandertal ancestry in East Asian than in European human populations. *Am. J. Hum. Genet.* **96**, 454–461 (2015).
6. Vernot, B. & Akey, J. M. Complex history of admixture between modern humans and Neandertals. *Am. J. Hum. Genet.* **96**, 448–453 (2015).
7. Villanea, F. A. & Schraiber, J. G. Multiple episodes of interbreeding between Neanderthal and modern humans. *Nat. Ecol. Evol.* **3**, 39–44 (2019).
8. Dannemann, M. & Kelso, J. The contribution of Neanderthals to phenotypic variation in modern humans. *Am. J. Hum. Genet.* **101**, 578–589 (2017).
9. Gittelman, R. M. et al. Archaic hominin admixture facilitated adaptation to out-of-Africa environments. *Curr. Biol.* **26**, 3375–3382 (2016).
10. Gregory, M. D. et al. Neanderthal-derived genetic variation shapes modern human cranium and brain. *Sci. Rep.* **7**, 6308 (2017).
11. McCoy, R. C., Wakefield, J. & Akey, J. M. Impacts of Neanderthal-introgressed sequences on the landscape of human gene expression. *Cell* **168**, 916–927 (2017).
12. Dannemann, M., Prüfer, K. & Kelso, J. Functional implications of Neandertal introgression in modern humans. *Genome Biol.* **18**, 61 (2017).
13. Simonti, C. N. et al. The phenotypic legacy of admixture between modern humans and Neandertals. *Science* **351**, 737–741 (2016).
14. Vernot, B. & Akey, J. M. Resurrecting surviving Neandertal lineages from modern human genomes. *Science* **343**, 1017–1021 (2014).
15. Sankararaman, S. et al. The genomic landscape of Neanderthal ancestry in present-day humans. *Nature* **507**, 354–357 (2014).
16. Steinrücken, M., Spence, J. P., Kamm, J. A., Wieczorek, E. & Song, Y. S. Model-based detection and analysis of introgressed Neanderthal ancestry in modern humans. *Mol. Ecol.* **27**, 3873–3888 (2018).
17. Meyer, M. et al. A high-coverage genome sequence from an archaic Denisovan individual. *Science* **338**, 222–226 (2012).
18. Prüfer, K. et al. The complete genome sequence of a Neanderthal from the Altai Mountains. *Nature* **505**, 43–49 (2014).
19. Slon, V. et al. The genome of the offspring of a Neanderthal mother and a Denisovan father. *Nature* **561**, 113–116 (2018).
20. Skov, L. et al. Detecting archaic introgression using an unadmixed outgroup. *PLoS Genet.* **14**, e1007641 (2018).
21. Kong, A. et al. Detection of sharing by descent, long-range phasing and haplotype imputation. *Nat. Genet.* **40**, 1068–1075 (2008).
22. The 1000 Genomes Project Consortium. A global reference for human genetic variation. *Nature* **526**, 68–74 (2015).
23. Sankararaman, S., Mallick, S., Patterson, N. & Reich, D. The combined landscape of Denisovan and Neanderthal ancestry in present-day humans. *Curr. Biol.* **26**, 1241–1247 (2016).
24. Vernot, B. et al. Excavating Neandertal and Denisovan DNA from the genomes of Melanesian individuals. *Science* **352**, 235–239 (2016).
25. Schumer, M. et al. Natural selection interacts with recombination to shape the evolution of hybrid genomes. *Science* **360**, 656–660 (2018).
26. Harris, K. & Pritchard, J. K. Rapid evolution of the human mutation spectrum. *eLife* **6**, e24284 (2017).
27. Moorjani, P., Amorim, C. E. G., Arndt, P. F. & Przeworski, M. Variation in the molecular clock of primates. *Proc. Natl Acad. Sci. USA* **113**, 10607–10612 (2016).
28. Jónsson, H. et al. Parental influence on human germline de novo mutations in 1,548 trios from Iceland. *Nature* **549**, 519–522 (2017).
29. Harris, K. & Nielsen, R. The genetic cost of Neanderthal introgression. *Genetics* **203**, 881–891 (2016).
30. Juric, I., Aeschbacher, S. & Coop, G. The strength of selection against Neanderthal introgression. *PLoS Genet.* **12**, e1006340 (2016).
31. Castellano, S. et al. Patterns of coding variation in the complete exomes of three Neandertals. *Proc. Natl Acad. Sci. USA* **111**, 6666–6671 (2014).
32. McLaren, W. et al. The Ensembl Variant Effect Predictor. *Genome Biol.* **17**, 122 (2016).
33. Sveinbjornsson, G. et al. Weighting sequence variants based on their annotation increases power of whole-genome association studies. *Nat. Genet.* **48**, 314–317 (2016).
34. Kote-Jarai, Z. et al. Identification of a novel prostate cancer susceptibility variant in the *KLK3* gene transcript. *Hum. Genet.* **129**, 687–694 (2011).
35. Hajdinjak, M. et al. Reconstructing the genetic history of late Neanderthals. *Nature* **555**, 652–656 (2018).
36. Besenbacher, S., Hvilsom, C., Marques-Bonet, T., Mailund, T. & Schierup, M. H. Direct estimation of mutations in great apes reconciles phylogenetic dating. *Nat. Ecol. Evol.* **3**, 286–292 (2019).

Methods

No statistical methods were used to predetermine sample size. The experiments were not randomized and the investigators were not blinded to allocation during experiments and outcome assessment. A detailed description of all analyses carried in this study out is included in the Supplementary Information.

Ethics statement

We used all of the samples (whole-genome sequenced and imputed, $n = 27{,}566$) available at deCODE Genetics at the time the study started. Recruitment is based on volunteers providing samples for particular disease and/or control studies either directly or through clinical collaborators. The study was undertaken on the basis of approvals from the National Bioethics Committee and the Icelandic Data Protection Authority. Blood or buccal samples were taken from individuals who participated in various studies, after receiving informed consent from the participants or their guardians.

Reporting summary

Further information on research design is available in the Nature Research Reporting Summary linked to this paper.

Data availability

All summary statistics such as archaic fragments and which SNPs they contain are available as Supplementary Data. Because Icelandic law and the regulations of the Icelandic Data Protection Authority prohibit the release of individual level and personally identifying data, collaborators who want access to individual genotype level data have to access the data locally at our Icelandic facilities.

Code availability

The Python script for performing simulations is available on Github (https://github.com/LauritsSkov/ArchaicSimulations).

Acknowledgements We thank K. Pruefer, B. Vernot, B. Peter, J. Kelso and S. Pääbo for comments on an earlier version of the manuscript. The study was supported by grant NNF18OC0031004 from the Novo Nordisk Foundation and grant 6108-00385 from the Research Council of Independent Research.

Author contributions L.S., M.C.M. and G.S. analysed the data with input from H.J., B.H., D.F.G., A.H. and M.H.S. L.S. and M.C.M. created the methods for analysing the data. L.S., M.C.M., A.H., F.M., K.S. and M.H.S. designed the study. L.S., M.C.M., A.H. and M.H.S. wrote the manuscript with input from all authors.

Competing interests All of the authors (except for L.S., M.C.M., F.M., E.A.L. and M.H.S.) are employees of deCODE Genetics and Amgen.

Additional information
Supplementary information is available for this paper at https://doi.org/10.1038/s41586-020-2225-9.
Correspondence and requests for materials should be addressed to L.S., M.H.S. or K.S.
Peer review information *Nature* thanks Stephan Schiffels and the other, anonymous, reviewer(s) for their contribution to the peer review of this work.
Reprints and permissions information is available at http://www.nature.com/reprints.

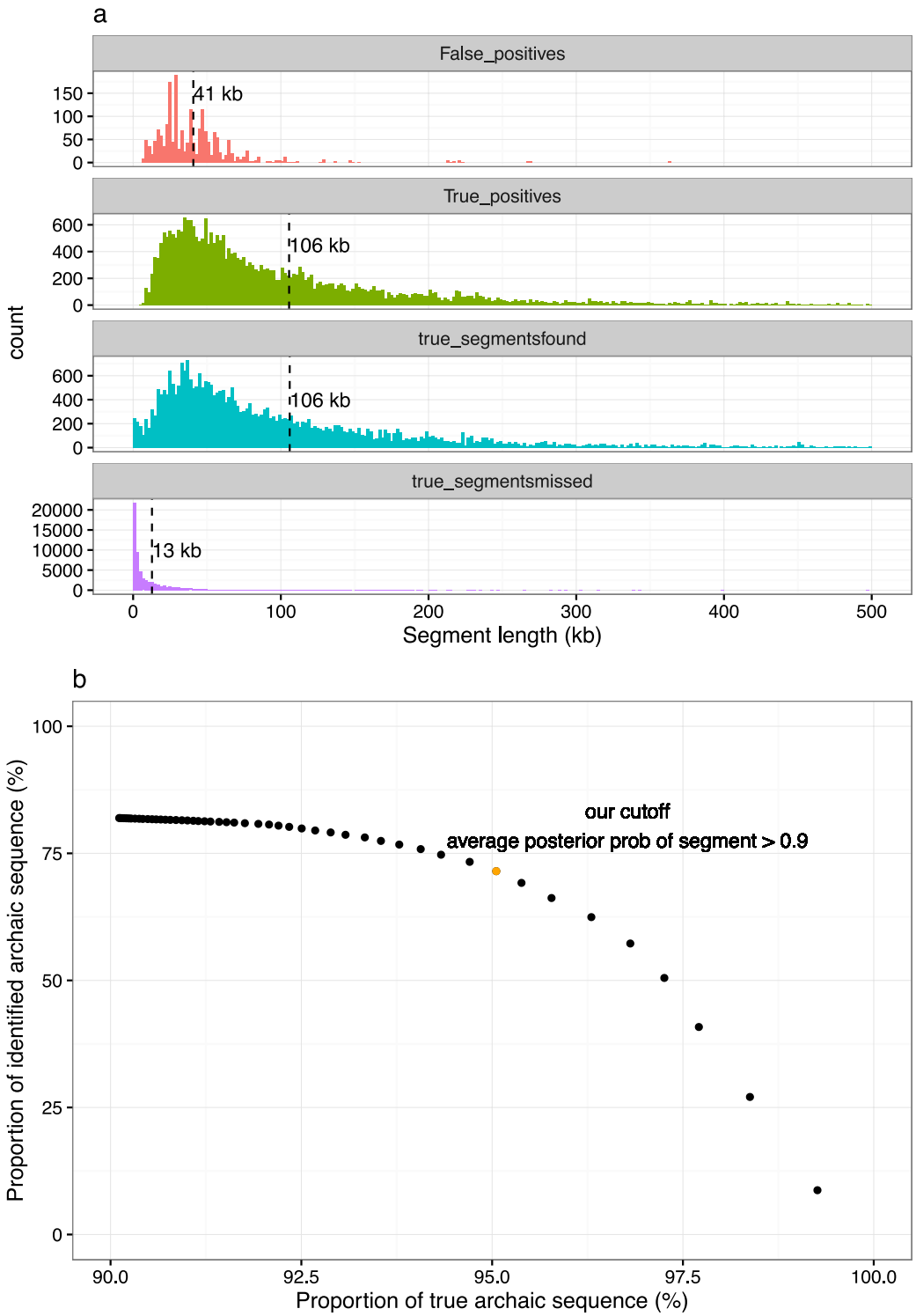

Extended Data Fig. 1 | Estimates of the false-positive rate of archaic inference based on simulations. a, Length distributions of false-positive and true-positive calls for fragments inferred to be archaic, and the length distributions for simulated archaic fragments that were found and those that were missed. The dashed lines indicate the mean value of the distribution. **b**, False-positive rate as a function of the mean posterior probability of being archaic for each fragment.

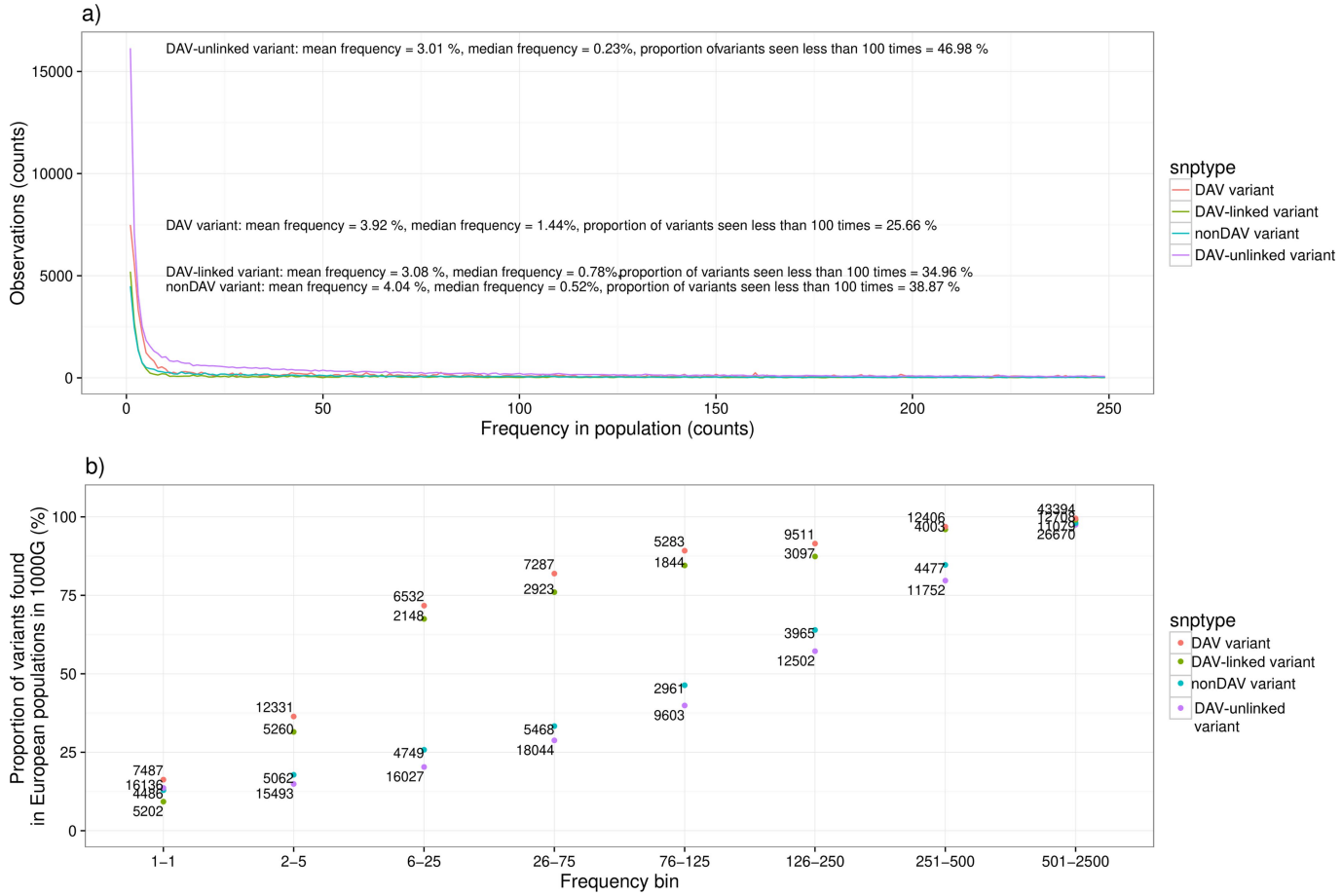

Extended Data Fig. 2 | Properties of SNP classes in archaic fragments. a, The site frequency spectrum for DAV variants, DAV-linked variants, DAV-unlinked variants and non-DAV variants. The *x* axis shows variants found on 1–250 chromosomes in our Icelandic population sample and the *y* axis shows the number of variants in each category. **b**, The number of times a variant is found in European populations (Utah residents (CEPH) with northern and western European ancestry (CEU), Toscani in Italy (TSI), Finnish in Finland (FIN), British in England and Scotland (GBR) and Iberian population in Spain (IBS); codes as per the previous study) from the 1000 Genomes Project (1000G) as a function of the number of times it is observed in Iceland. The numerical labels represent the number of variants that belong to each category defined by the two axes and the type of archaic variant. The *x* axis is truncated at variants that were found 2,500 times, which corresponds to a frequency of around 5% in Iceland.

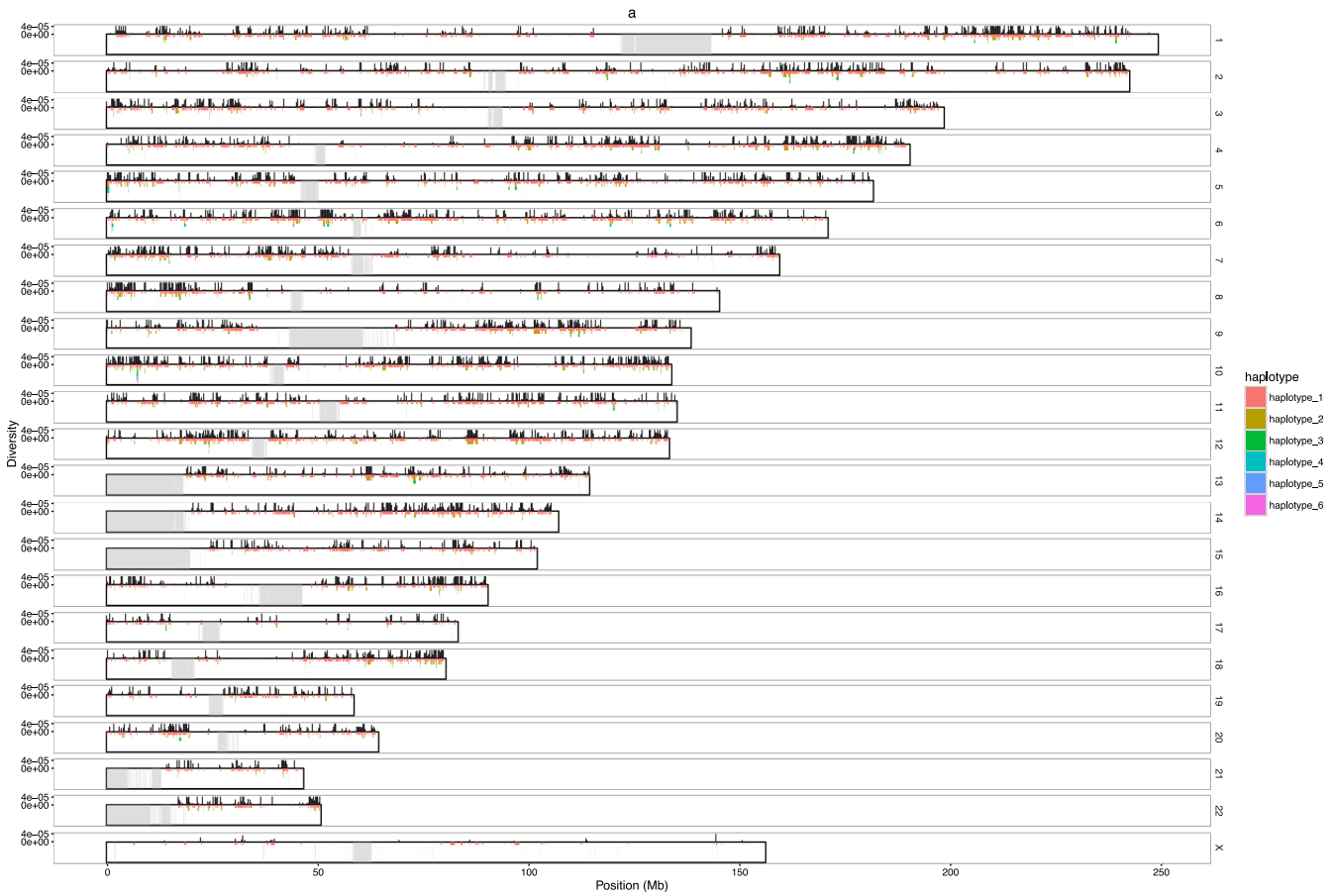

Extended Data Fig. 3 | Nucleotide diversity based on DAV-linked and DAV variants from archaic fragments. Using these variants, we identified a maximum of 6 subgroups of fragments, clustered by similarity (based on a mean difference of 1 mismatch per 10 kb per subgroup).

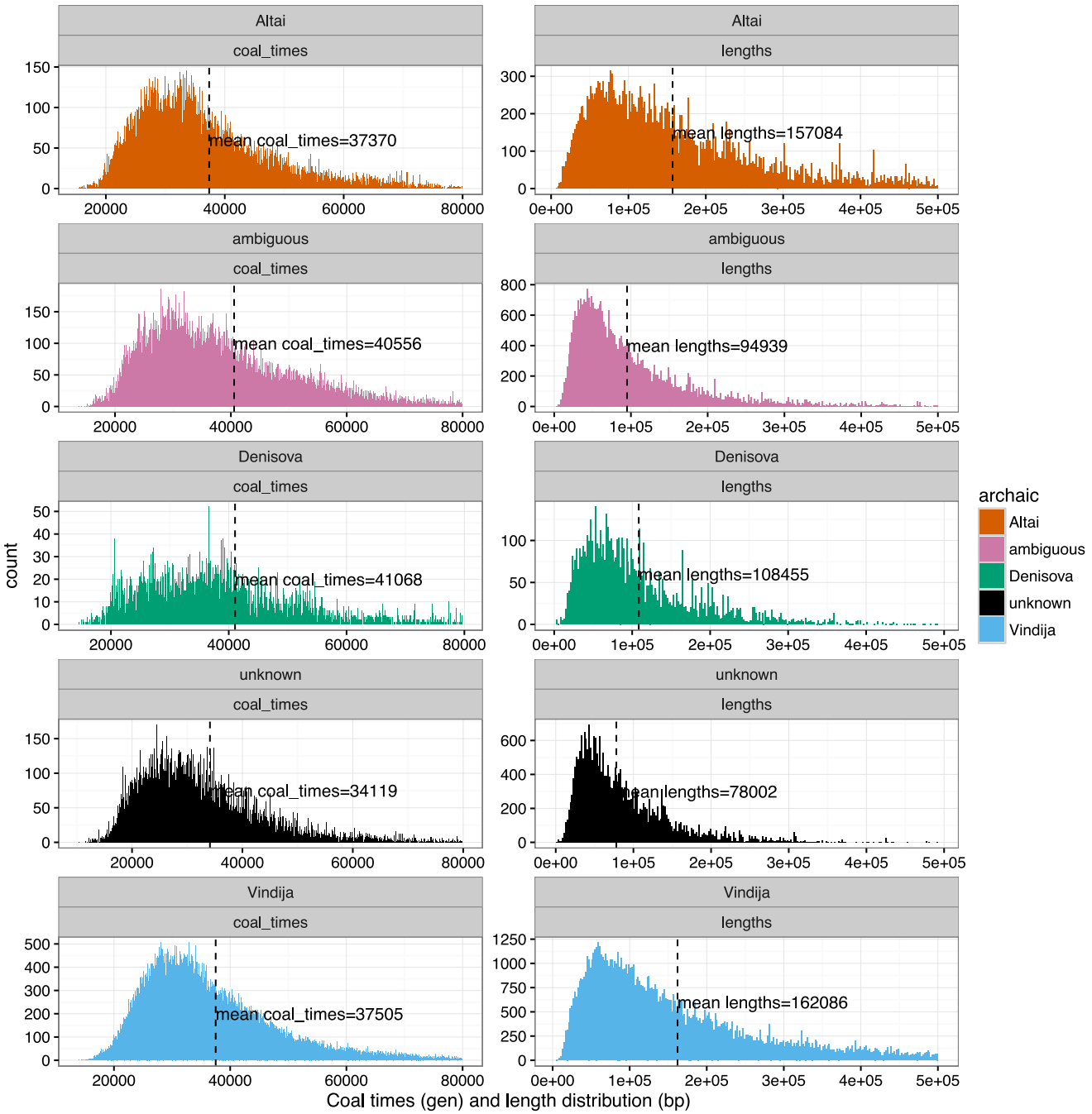

Extended Data Fig. 4 | Length distribution and coalescence time for all archaic fragments. The distribution of length and coalescence times (with present day sub-Saharan Africans) for all archaic fragments (mosaic and non-mosaic) are shown according to the archaic genome that they are most closely related to (Altai, Denisova, Vindija, multiple archaics (ambiguous) and unknown). The coalescence time estimates are described in Supplementary Information 2.7.

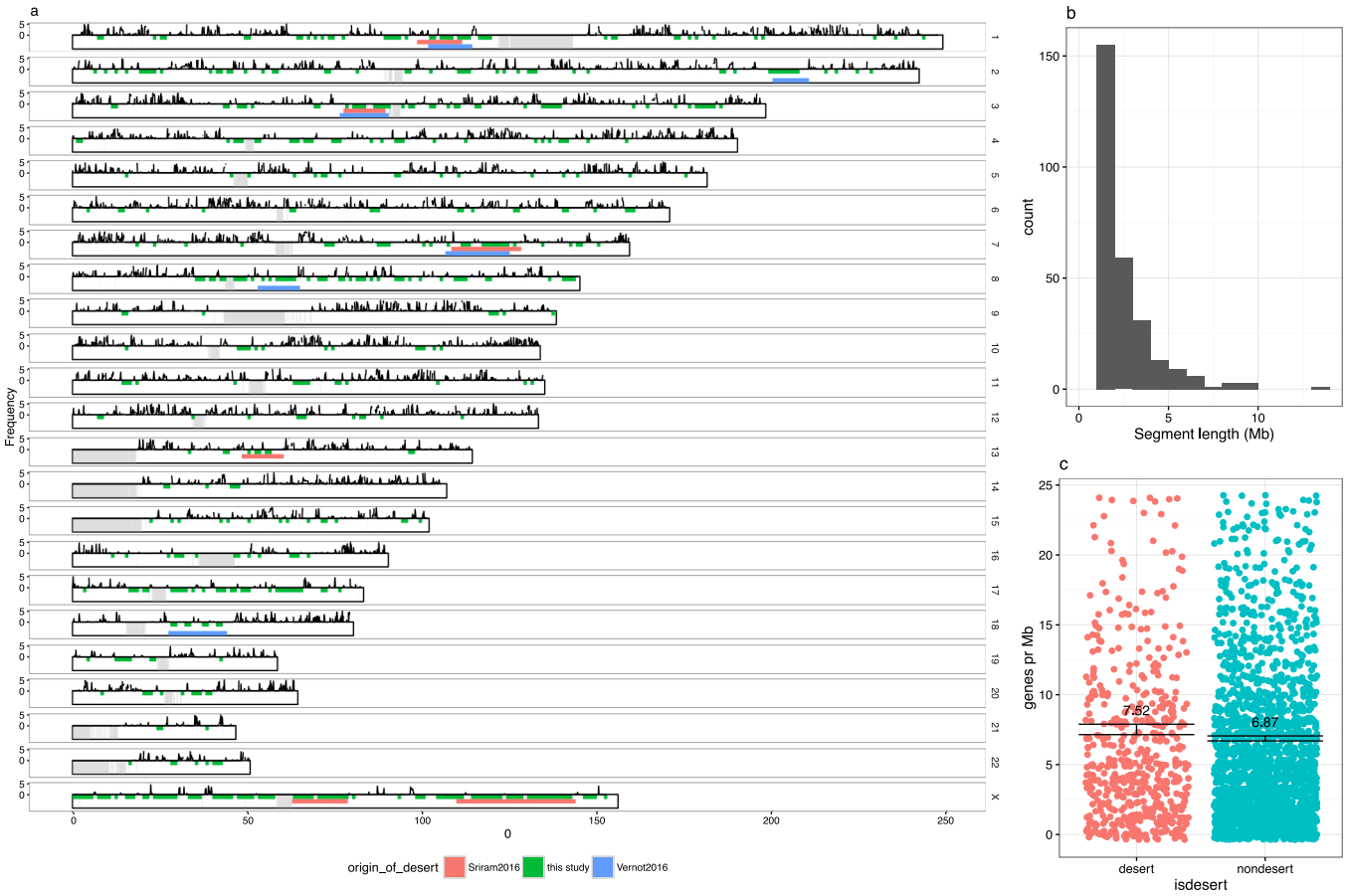

Extended Data Fig. 5 | A genomic map of archaic introgression deserts. **a**, The mean frequency of archaic fragments in each 100-kb bin is reported along the genome (ideogram). The *y* axis is truncated at 5%. Regions with no archaic fragments (only counting fragments with DAV variants and DAV-linked variants) in regions larger than 1 Mb (and a minimum of 100 kb could be called) are marked in green, along with previously reported deserts in red[23] and blue[24]. **b**, The size distribution of archaic introgression deserts. **c**, Gene density in deserts ($n = 570$) compared with non-deserts ($n = 2,224$). The numbers indicate the mean number of genes per Mb and the error bars are 95% confidence intervals. The *y* axis is truncated at 25 genes per Mb.

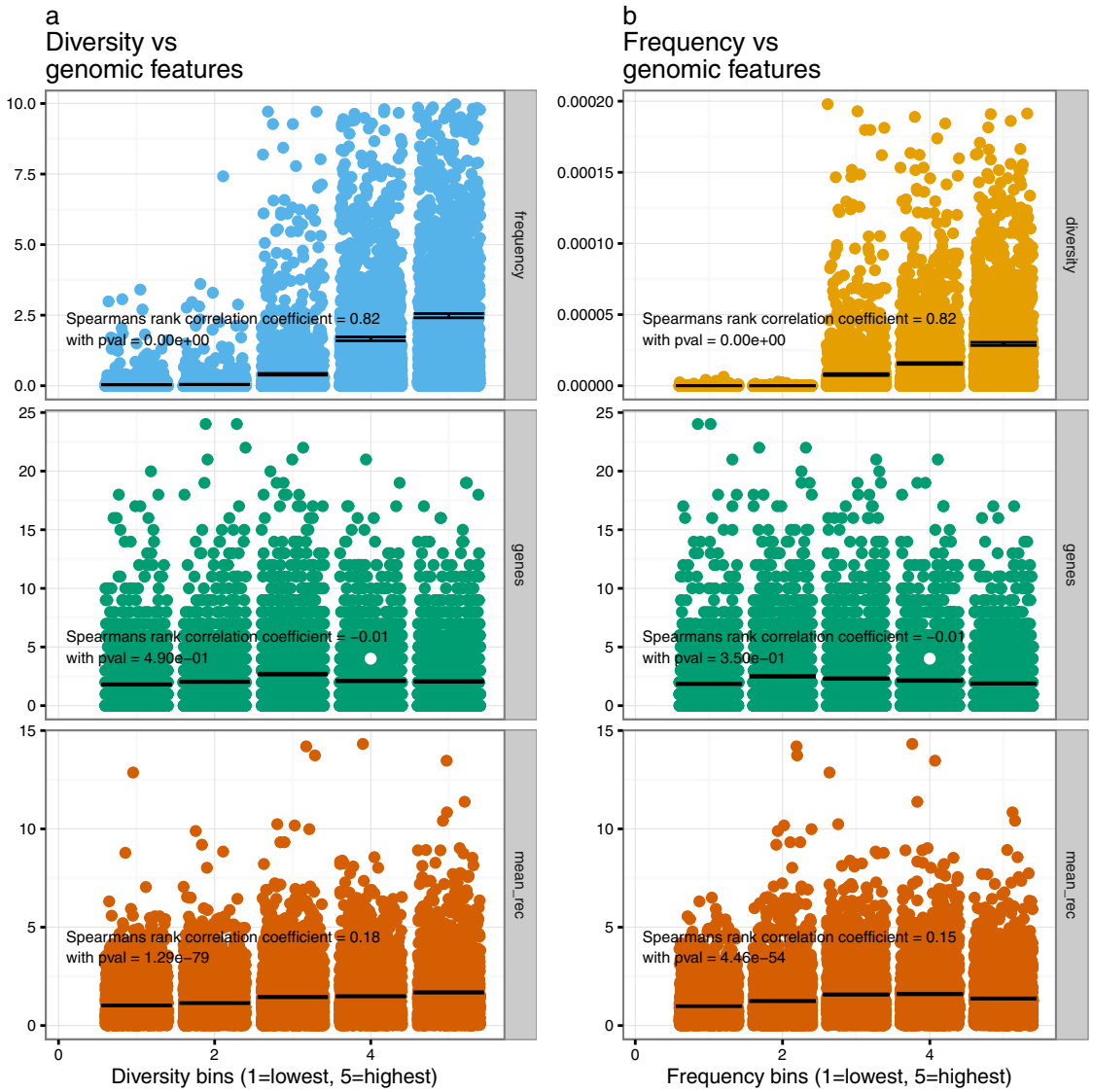

Extended Data Fig. 6 | Archaic introgression and genomic features in 250-kb windows for which more than 1% of the bases in the window could be called. $n = 10{,}466$. **a**, **b**, The relationship between the nucleotide diversity of archaic fragments (**a**) or their frequency (%) (**b**) and the recombination rate (cM per Mb) and gene density (number of genes per 250 kb). Data were analysed by Spearman's rank correlation coefficient and *P* values for all data points (two-sided test) are shown. For visualization, we group the data into five equally sized bines, sorted by diversity (**a**) or frequency (**b**). Each bin contains 2,093 data points. In this analysis, we considered only DAV-linked variants and DAV variants. The data are coloured according to which feature is being tested (blue for frequency, orange for genes, green for recombination rate and yellow for diversity). The midpoint of the bar is the mean of the measure and error bars are 95% confidence intervals. The *y* axis is truncated at five times the mean value.

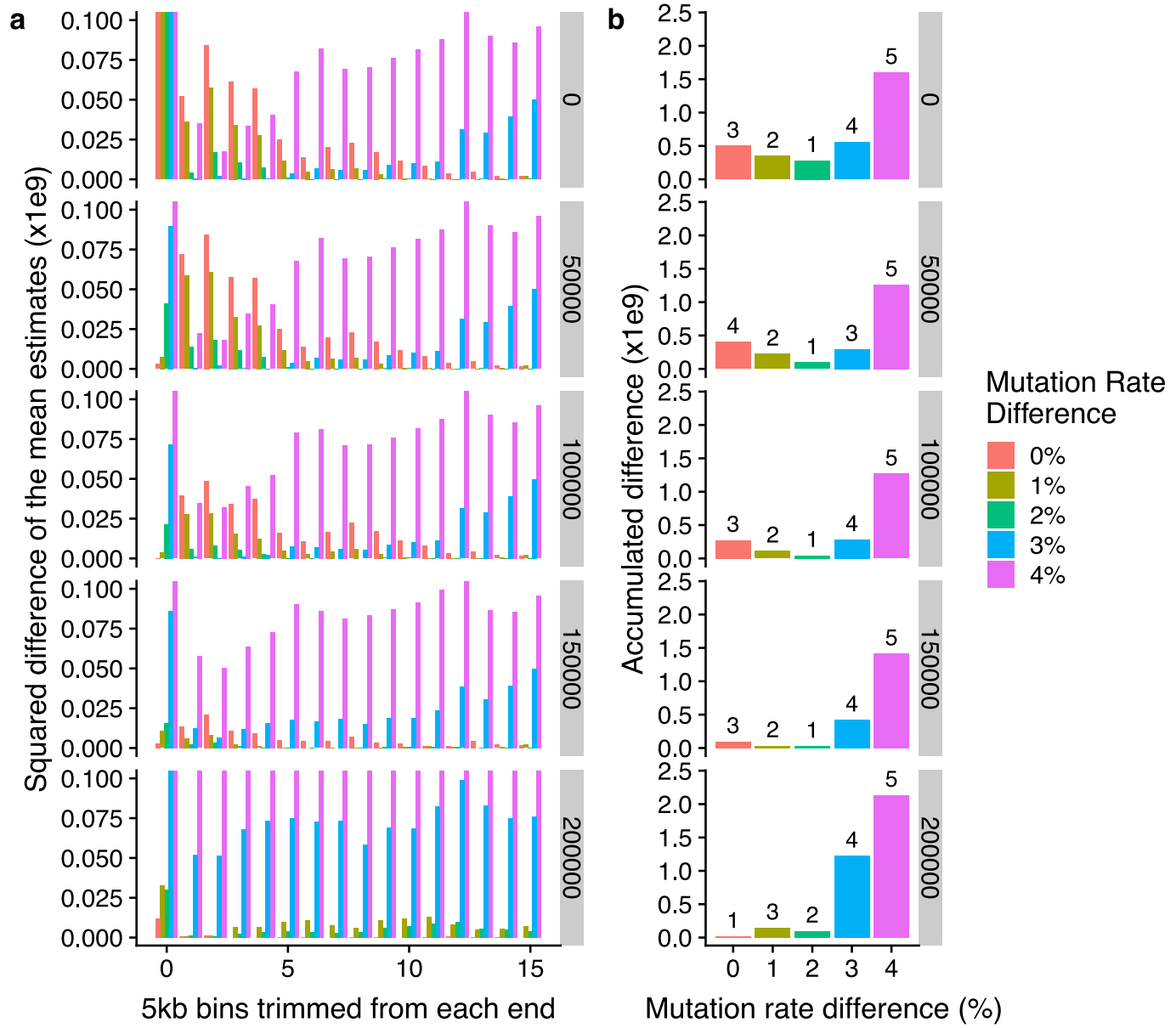

Extended Data Fig. 7 | Difference between observed and simulated fragments based on increasing Neanderthal-to-human mutation rates. **a**, The square-root difference of the 10-replicate mean simulated scenarios for Δ_{AH} (difference scenarios have mutation rates of 0, 1, 2, 3 and 4%) and the observed values of Δ_{AH} for the Icelandic fragments, after trimming different numbers of 5-kb bins from the ends of each fragment. The analysis was repeated applying 0-, 50-, 100-, 150- and 200-kb minimum fragment length filters (facets). **b**, As in **a**, but adding up the square-root difference value for all the bins trimmed and ranking each bar by the minimum difference (number on top of each bar: 1, minimum difference; 5, maximum difference).

nature research

Corresponding author(s): Laurits Skov

Last updated by author(s): Feb 8, 2020

Reporting Summary

Nature Research wishes to improve the reproducibility of the work that we publish. This form provides structure for consistency and transparency in reporting. For further information on Nature Research policies, see Authors & Referees and the Editorial Policy Checklist.

Statistics

For all statistical analyses, confirm that the following items are present in the figure legend, table legend, main text, or Methods section.

n/a	Confirmed	
☐	☒	The exact sample size (*n*) for each experimental group/condition, given as a discrete number and unit of measurement
☐	☒	A statement on whether measurements were taken from distinct samples or whether the same sample was measured repeatedly
☐	☒	The statistical test(s) used AND whether they are one- or two-sided *Only common tests should be described solely by name; describe more complex techniques in the Methods section.*
☐	☒	A description of all covariates tested
☐	☒	A description of any assumptions or corrections, such as tests of normality and adjustment for multiple comparisons
☐	☒	A full description of the statistical parameters including central tendency (e.g. means) or other basic estimates (e.g. regression coefficient) AND variation (e.g. standard deviation) or associated estimates of uncertainty (e.g. confidence intervals)
☐	☒	For null hypothesis testing, the test statistic (e.g. *F*, *t*, *r*) with confidence intervals, effect sizes, degrees of freedom and *P* value noted *Give P values as exact values whenever suitable.*
☒	☐	For Bayesian analysis, information on the choice of priors and Markov chain Monte Carlo settings
☒	☐	For hierarchical and complex designs, identification of the appropriate level for tests and full reporting of outcomes
☐	☒	Estimates of effect sizes (e.g. Cohen's *d*, Pearson's *r*), indicating how they were calculated

Our web collection on statistics for biologists contains articles on many of the points above.

Software and code

Policy information about availability of computer code

Data collection	The description of the data acquisition and processing is described in the Data Descriptor (Jónsson, H. et al. Whole genome characterization of sequence diversity of 15,220 Icelanders. Sci. Data 4:170115 doi: 10.1038/sdata.2017.115 (2017).)
Data analysis	Custom scripts written in python 2.7 Bedtools v2.25.0-76-g5e7c696z, https://github.com/arq5x/bedtools2/ Msprime v0.4.0 Scipy v1.3.1

For manuscripts utilizing custom algorithms or software that are central to the research but not yet described in published literature, software must be made available to editors/reviewers. We strongly encourage code deposition in a community repository (e.g. GitHub). See the Nature Research guidelines for submitting code & software for further information.

Data

Policy information about availability of data

All manuscripts must include a data availability statement. This statement should provide the following information, where applicable:

- Accession codes, unique identifiers, or web links for publicly available datasets
- A list of figures that have associated raw data
- A description of any restrictions on data availability

Icelandic law and the regulations of the Icelandic Data Protection Authority prohibit the release of individual level and personally identifying data. We are actively participating in multiple meta-analysis based on our data and are in collaboration with groups at over 100 international universities and institutions. Therefore, collaborations based on our sequencing data are based on the release of summary level statistics, such as effect sizes and P-values for meta-analysis, or the collaborators travelling to our Icelandic facilities for local data access.

Field-specific reporting

Please select the one below that is the best fit for your research. If you are not sure, read the appropriate sections before making your selection.

☒ Life sciences ☐ Behavioural & social sciences ☐ Ecological, evolutionary & environmental sciences

For a reference copy of the document with all sections, see nature.com/documents/nr-reporting-summary-flat.pdf

Life sciences study design

All studies must disclose on these points even when the disclosure is negative.

Sample size	27566
Data exclusions	We excluded 268 individuals with low callability (less than 7,000,000 genotyped variants per genome). These variants were excluded because no introgressing archaic fragments could be identified.
Replication	We compare to other methods used for detecting archaic introgression (Supplementary section 2.4). We compare introgressed archaic tracks found in parent-offspring pairs and found a mean concordance between fragments of 99.63 (median=100)
Randomization	The experiments were not randomized
Blinding	The investigators were not blinded to allocation during experiments and outcome assessment.

Reporting for specific materials, systems and methods

We require information from authors about some types of materials, experimental systems and methods used in many studies. Here, indicate whether each material, system or method listed is relevant to your study. If you are not sure if a list item applies to your research, read the appropriate section before selecting a response.

Materials & experimental systems

n/a	Involved in the study
☒	☐ Antibodies
☒	☐ Eukaryotic cell lines
☒	☐ Palaeontology
☒	☐ Animals and other organisms
☐	☒ Human research participants
☒	☐ Clinical data

Methods

n/a	Involved in the study
☒	☐ ChIP-seq
☒	☐ Flow cytometry
☒	☐ MRI-based neuroimaging

Human research participants

Policy information about studies involving human research participants

Population characteristics	We used all of the available samples 27566 (whole genome sequenced and imputed) at deCODE Genetics at the time the study was started. There are no covariate-relavant population characteristics of the human research participants.
Recruitment	Recruitment is based on volunteers providing samples for particular disease and/or control studies either directly or through clinical collaborators. We are not aware of any recruitment biases that would impact the results of this study
Ethics oversight	The study is undertaken on the basis of approvals from the National Bioethics Committee and the Icelandic Data Protection Authority. Blood or buccal samples were taken from individuals participating in various studies, after receiving informed consent from them or their guardians.

Note that full information on the approval of the study protocol must also be provided in the manuscript.